Phenomenological modelling of polymer crystallization using the notion of multiple natural configurations

I. J. RAO AND K. R. RAJAGOPAL

Department of Mechanical Engineering, Texas A&M University, College Station, TX 77843, USA

Crystallization and solidification in polymers is a problem of great importance to the polymer processing industry. In these processes, the melt is subjected to deformation while being cooled into the desired shape. The properties of the final product are strongly influenced by the deformation and thermal histories and the final solid is invariably anisotropic. In this work we present a model to capture the effects during solidification and crystallization in polymers within a purely mechanical setting, using the framework of multiple natural configurations that was introduced recently to study a variety of non-linear dissipative responses of materials undergoing phase transitions. Using this framework we present a consistent method to model the transition from a fluid-like behaviour to a solid-like behaviour. We also present a novel way of incorporating the formation of an anisotropic crystalline phase in the melt. The anisotropy of the crystalline phase, and consequently that of the final solid, depends on the deformation in the melt at the instant of crystallization, a fact that has been known for a long time and has been exploited in polymer processing. The proposed model is tested by solving three homogenous deformations.

1. Introduction

The mechanical behaviour of polymeric materials is intimately related to the polymer structure and morphology. The key aspects of a polymer's structure include its molecular weight, molecular weight distribution and the organization and composition of atoms down the polymer chain. The morphology of polymeric materials is highly variable. Many polymers are semi-crystalline, and the shape, size, crystallinity and organization of the crystallites depend on the conditions under which the crystallization took place. Other polymers are amorphous, often because their chains are too irregular to permit regular packing.

The majority of plastic products are manufactured by heating the polymer to above its melting temperature and then cooling it in a mould (e.g. injection moulding) or subjecting the melt to deformation while simultaneously cooling it to achieve the desired shape (e.g. film blowing and fibre spinning). The properties of the final product strongly depend on the processing conditions the polymer is subjected to during manufacture, for e.g., in the case of film blowing the crystalline orientation depends on the amount of stretch imparted in the machine direction and the transverse direction. Bi-axial extension strengthens the film in the plane, due to which films find widespread use as packaging materials. Uni-axial extension of melts is used to form high-strength fibres, in these fibres the polymer molecules crystallize with their backbone parallel to the fibre direction. The successful use of polyester bottles for carbonated drinks was made possible by the development of a special blow moulding process that ensures that the polymer in the bottle is bi-axially oriented. The surface layer of an injection moulded article is highly oriented; this has a negative influence on the product quality, resulting in products that are easily cleaved. The above examples illustrate the

importance of understanding the phase transition from the melt to a semi-crystalline or amorphous solid as it determines the properties of the final product. In this section we provide a review of the different efforts to model phase transitions with an emphasis on crystallization in polymers. This does not purport to be an exhaustive review.

Polymer melts are generally modelled as isotropic viscoelastic liquids (see Doi & Edwards [12] and Astarita and Marucci [2]). Depending on the molecular structure and processing conditions, the final solid can either be in an amorphous or semi-crystalline state. Polymers that are unable to crystallize, on cooling to below their glass transition temperature form amorphous solids. These amorphous solids can have anisotropy[†] in the mechanical behaviour if the melt is subjected to deformation while cooling below the glass transition temperature. As the deformed amorphous polymer cools below its glass transition temperature, the molecules lose their mobility and are 'frozen' in this oriented configuration. Polymers having a regular molecular structure, when kept at temperatures below the melting temperature for a sufficiently long time, form a semi-crystalline solid. Under quiescent conditions, the crystallization process is very slow and the solid has a spherulitic morphology. The rate of crystallization strongly depends on the molecular orientation in the melt. Subjecting the melt to deformations that align the molecules dramatically increases the rate of crystallization. When the temperature falls below the glass transition temperature, there is a cessation of molecular motion and the crystallization process halts. The crystallization process also halts as the crystallinity increases, decreasing the mobility of the polymer molecule in the amorphous fraction. A number of polymeric solids like polyethylene find applications at temperatures between their melting temperature and glass transition temperature. At these temperatures, the solid consists of rigid crystals and a flexible amorphous fraction resulting in a solid that is both flexible and tough. The mechanical properties of the final product are strongly dependent on the final morphology of the amorphous and semi-crystalline regions. The morphology, in turn, is a function of the thermal and deformation history undergone by the material during processing.

The early work on phase transitions was devoted to analysing problems where conduction was the dominant mechanism. Such studies can be traced back to the works of Lamé & Clayperon [29] and Stefan [56], in which temperature is considered to be the basic variable (see Crank [11], Fasano & Primicerio [15], Bankoff [8] and Rubinstein [51]) Another popular approach is the 'Phase-Field' model which involves another parameter (other than temperature) called the order parameter. The order parameter has extreme values of $+1$ (for pure liquid) and -1 (for pure solid). The heat conduction equation is modified to incorporate the effect of the order parameter that leads to an additional equation whose origin can be traced back to the Landau–Ginzburg theory of phase transitions [30]. In most practical situations in which fluid to solid phase transitions take place, several other mechanisms other than conduction come into play, for e.g., convection in the liquid and deformation in the solid. This shortcoming is partially overcome by introducing a special kinematics for the fluid (see Glicksman *et al.* [19]); however, the forming solid is still assumed to be completely quiescent. This approach results in a model that cannot predict the structural and mechanical properties of the newly formed solid. The ability to predict the properties of the newly formed solid are however essential in all applications, especially so in polymers where

---

[†] Generally, the term amorphous is synonymous with the term isotropic. However, with regard to polymers, even though X-ray diffraction methods reveal no evidence of three-dimensional order, optical methods detect small differences in the refractive index in different directions. The structure of these may be regarded as a somewhat oriented, tangled collection of spaghetti-like molecules. Of course, this implies that the material is anisotropic with respect to optical properties. However, it is commonly observed that the body is also mechanically anisotropic. (see Ward & Hadley [60]).

the properties of the final solid depend strongly on the processing conditions. Solid–liquid phase transitions present additional challenges as there is a discontinuous transition in the symmetry of the material. Since the issue of symmetry enters the problem only when the kinematical fields of the fluid and solid are taken into account, both the Stefan approach and the phase-field approach do not deal with one of the thorniest issues in phase transitions. Baldoni & Rajagopal [7] have developed a continuum theory for phase transitions, that can account for changes in symmetry. However, in the specific model developed they assume that the solid is isotropic and the response is like that for a neo-Hookean solid.

The condition under which the melt nucleates, its subsequent growth and its final equilibrium characterize the crystallization in polymers as in other solidifying systems. Nuclei develop either randomly or at impurities. These nuclei can either grow or are destroyed. New nuclei can be generated in uncrystallized regions of the melt. This process of nucleation and growth continues until crystals impinging on one another restrict the growth or growth is restricted due to constraints imposed by the amorphous region. The morphology of the solid formed under quiescent conditions is spherulitic. The traditional way to model crystallization in polymers is based on the work of Avrami ([4, 5, 6]). The Avrami equation that has been used widely in modelling quiescent crystallization is based on the theory of filling space through the nucleation and growth of one phase into another. Different variations of the basic Avrami equation to account for isothermal and non-isothermal conditions can be found in a detailed review by Eder *et al.* [13]. Experimental correlations for Avrami's equations can be found in the text by Mandelkern [36]. Of course, it is possible within the framework of the theory presented here to assume a very general form for the equation that governs the crystallization kinetics.

The Stefan problem for polymer solidification has been studied by a number of researchers. In the classical Stefan problem, solidification of a semi-infinite pool of liquid is initiated by quenching the 'wall' at the origin. After quenching, a solidification front propagates into the melt. In polymers, however, crystallization takes place over a range of temperatures between the melting temperature and the glass transition temperature, resulting in diffuse crystallization in the melt, before the arrival of the solid phase boundary. Experimental evidence for this phenomenon has been reported by Krobath *et al.* [27], Janeschitz-Kriegl *et al.* [21] and Eder [13]. This problem has been modelled by a number of researchers by combining the crystallization kinetics equations, similar to the Avrami equation, with the transient heat conduction equation (see Malkin *et al.* [34, 35], Berger & Schneider [9], Eder [13] and Astarita & Kenny [1]). This approach is similar to the phase-field approach.

As the process of crystallization of polymeric melts is quite complicated depending on a plethora of quantities, we shall try to provide some details concerning experimental studies of crystallization. In most practical processes, crystallization rarely takes place under quiescent conditions. When the phase transition takes place in a flowing polymer melt, the morphology of the final solid depends on the temperature and deformation history. Crystallization under flow conditions increases the rate of crystallization by orders of magnitude (see Haas & Maxwell [20], Lagasse & Maxwell [28], Eder *et al.* [13] and McHugh [37]). Usually, a highly oriented row-nucleated crystalline morphology is obtained (Keller & Machin [25], Kawai *et al.* [24]) in contrast to the spherulitic morphology observed under conditions of quiescent crystallization. The effect of different polymer processes on the orientation and morphology has been widely studied (see Peterlin [40], White [61] and White & Spruiell [62]). In spun fibres the lamellae are found to be perpendicular to the fibre axis and in the case of blown film the lamellae are distributed in the plane of the film. The outer layer of injection moulded articles has lamellae oriented perpendicular to both the surface and injection directions

while the interior is spherulitic, in the intermediate layers the lamellae remain perpendicular to the surface but lose their preferred orientation with respect to the direction of injection.

A number of experiments have been conducted concerning crystallization in sheared polymer melts. One of the early experiments on crystallization in simple shear flow between parallel plates was carried out by Haas & Maxwell [20]. In their experiments, tiny samples of polyethylene and polybutene-1 (less than 0.5 mm thick) were sheared between two parallel glass plates by applying a constant load under isothermal conditions at a temperature below the melting point. At low loads spherulitic growth was observed, while at sufficiently high loads flow-induced crystallization was so profuse that no textural detail was observed in the polarizing microscope. Also, the time required for crystallization was orders of magnitude less than that for quiescent crystallization. Similar experiments have been performed by Katayama *et al*. [23], Nogami *et al*. [39] and Lagasse & Maxwell [28]. Lagasse & Maxwell [28] performed the experiment under conditions of constant shear rate instead of constant load. At low shear rates spherulitic crystallization was observed and at higher shear rates flow induced crystallization was observed, the two regions being clearly demarcated. Enhanced crystallization was determined to be due to chain extension arising from entanglements between molecules. Flow-induced crystallization has also been studied in rotational viscometers (see Kobayashi & Nagasawa [26], Ulrich & Price [58], Sherwood *et al*. [53] and Wolcowicz [63]), the results are similar to those obtained from simple shear experiments.

Experiments on flow-induced crystallization have also been performed in ducts of rectangular cross-section (see Eder *et al*. [14]). This is very similar to injection moulding, where one finds highly oriented surface layers which appear due to flow-induced crystallization. In this work polypropylene was extruded in a channel, the exiting fluid tape was either laid directly on a chill roll or was placed on a heated conveyor belt and was chilled at some length from the exit of the duct. The main conclusion of this work was that the relaxation time of the melt has a strong impact on the final thickness of the highly oriented surface layer. When the melt was allowed to relax on the heated conveyor belt at a high temperature after exit from the extruder, the thickness of the surface layer decreased rapidly with increasing residence time on the belt. For sufficiently high residence times this layer was negligible in thickness. This effect diminished significantly when the temperature of the heated conveyor belt was lowered, i.e. at lower conveyor belt temperatures the thickness of the surface layer did not decrease as rapidly with an increase in the residence time on the heated belt.

Experiments in extensional flows are not as numerous as in shear flows, the main reason being the extreme sensitivity of crystallization to extensional flow, often resulting in flow blockage due to massive crystallization (see van der Vegt & Smit [59]). Early work on extensional flows was carried out by Mackley & Keller [32] and Mackley *et al*. [33], and they reported qualitative rheo-optical characteristics of extensional flow induced crystallization in a confined geometry. In a more recent paper, McHugh *et al*. [37] studied the crystallization of polyethylene in extensional flows by suspending a high-density polyethylene droplet at the stagnation point of a four-roll mill extensional device with linear low-density polyethylene as the carrier phase. The crystallization rate was enhanced by orders of magnitude and the accompanying analysis demonstrates that the melting point elevation model cannot predict the phenomena observed.

Flow induced crystallization in melts has been modelled from two main perspectives. The classical work of Flory [16] on the stress-induced crystallization of rubber has been used to model crystallization from melts. Extension of Flory's work to melts requires the assumption that the temporary network junctions play the same role as the chemical cross-links in the theory of rubber crystallization. Flory's theory rests on the connection between decrease in entropy of the

stretched molecule and the tendency of the polymer to crystallize. This work by Flory has been extended by deriving more complicated expressions for the Helmholtz potential which describe the morphological effects in greater detail (see Gaylord & Lohse [17], Gaylord [18], Smith [54] and Smith [55]). In polymer melts, however, the relaxation time of the melt has a strong influence on the crystallization. Melts with long relaxation times will experience higher amounts of crystallization compared with ones having a shorter relaxation time. All the theories developed for the crystallization of rubber do not account for relaxation effects of the network. The other approach to model flow induced crystallization is to modify the Avrami equation to account for enhanced crystallization rates due to the flow. In this approach, the effect of flow is built into the equation by the inclusion of an orientation factor, which depends on the flow (see Ziabicki [64], [65], Eder [13] and Schultz [52]).

From the experiments performed on phase transitions in polymers that crystallize, it is clear that the transition from a melt to a semi-crystalline solid is continuous, i.e. during this process the material is a mixture of an amorphous polymer melt and a crystalline solid. On the completion of crystallization the solid formed is a mixture of a crystalline and amorphous solid. Orientation in the melt tremendously accelerates the process of phase transition. However, as the melt is a viscoelastic fluid, the orientation of the molecules can either build up or relax depending on the deformation history and the relaxation time of the melt. Orientation of the crystallites formed depends strongly on the orientation of the molecules in the melt just prior to crystallization.

In this paper we model the phase transition process within a purely mechanical setting. A model for phase transitions in a purely mechanical setting is not adequate as thermodynamical issues dominate the phase transition process. The aim of this paper is to clarify the mechanical issues relating to phase transitions and describe a method to capture changes in symmetry of the newly formed solid. Previous work done on crystallization in polymers has primarily concentrated on ways to incorporate the effect of different variables like stress, temperature, etc. on the equation governing the rate of crystallization (see Ziabicki [64, 65], Eder [13] and Schultz [52]) in an ad hoc manner, not based on a criterion like, say, that the rate of dissipation or entropy production be maximized, etc. These papers are essentially concerned about the crystallization kinetics and invariably treat the solid as though it is a fluid with a large viscosity, or this transition from a fluid-like to a solid-like behaviour is ignored. More importantly, these works do not address the important issue of anisotropy in the mechanical response of the crystalline phase formed during crystallization and the role of the rate of dissipation in the evolution of the stress-free state of the material. As has been illustrated earlier, the anisotropy of the newly formed crystalline phase depends on the deformation history of the melt and the model developed here is able to capture this effect. We feel that it is important to explain these ideas in a clear manner without clouding the matter with other issues, especially since the changes of symmetry during solidification has not been tackled adequately. In this work a model is developed using a continuum theory based on the concept of 'multiple natural configurations' (see Rajagopal [41]). This approach has been used to explain the material response of a large class of materials under one framework: ligaments and tendons (Johnson *et al*. [22]), multi-network theory (Rajagopal & Wineman [42]), traditional plasticity (Rajagopal & Srinivasa [43]), twinning (Rajagopal & Srinivasa [44]), solid to solid phase transitions (Rajagopal & Srinivasa [45]), viscoelastic liquids (Rajagopal & Srinivasa [46]) and anisotropic liquids (Rajagopal & Srinivasa [47]) have all been modelled within this framework, and classical elasticity and classical linearly viscous fluids arise naturally as sub-cases. The melt is modelled as a viscoelastic fluid, within the framework of natural configurations as formulated by Rajagopal & Srinivasa [46]. In

this approach, the stress in the fluid depends on the mapping between the tangent spaces associated with the natural configuration and the current configuration. This mapping also contains information about the orientation of the polymer molecules, albeit in an averaged sense. Once the phase change is initiated, continuous conversion of the melt into a semi-crystalline solid takes place. This conversion is never complete in polymers. The newly formed crystalline phase is an anisotropic material and the anisotropy depends on the orientation of the molecules in the amorphous phase at the instant of crystallization. This is captured in the model by making the anisotropy in the crystalline solid depend on the mapping between the tangent spaces of the natural configuration and the current configuration of the melt. Crystallization ceases when molecules in the amorphous phase lose there mobility, this effect is captured by making the relaxation time of the melt increase with increasing crystallinity. For sufficiently large values of relaxation time the amorphous phase acts as an elastic solid. The final solid is a mixture of a crystalline and amorphous elastic solid. The model is tested for three different homogenous deformations, viz. simple extension, bi-axial extension and simple shear.

2. Preliminaries

Consider a body B in a configuration κ_0. Let $\mathbf{X}$ denote a typical position of a material point in κ_0. Let κ_t be the configuration at a time t, then the motion χ_{κ_0} assigns to each particle in configuration κ_0 a position in the configuration κ_t at time t, i.e.

$$\mathbf{x} = \chi_{\kappa_0}(\mathbf{X}, t). \tag{1}$$

The deformation gradient $\mathbf{F}_{\kappa_0}$ is defined through

$$\mathbf{F}_{\kappa_0} \equiv \frac{\partial \chi_{\kappa_0}}{\partial \mathbf{X}}. \tag{2}$$

The left and right Cauchy–Green stretch tensors $\mathbf{B}_{\kappa_0}$ and $\mathbf{C}_{\kappa_0}$ are defined through

$$\mathbf{B}_{\kappa_0} \equiv \mathbf{F}_{\kappa_0} \mathbf{F}_{\kappa_0}^T, \tag{3}$$

$$\mathbf{C}_{\kappa_0} \equiv \mathbf{F}_{\kappa_0}^T \mathbf{F}_{\kappa_0}. \tag{4}$$

The modelling of crystallization can be delineated into three main categories, viz. the modelling of the melt, the intermediate mushy region between a fluid and solid and finally the solid region. Constitutive assumptions have to be made for each of these regions.

3. Modelling

3.1 *Modelling the melt*

The melt is modelled as a viscoelastic fluid with instantaneous elasticity. It has been shown by Rajagopal & Srinivasa [46] that a viscoelastic fluid that is capable of instantaneous elastic response can be described within the context of a material with evolving natural configurations. A large number of viscoelastic fluid models can be written in this form (see Rajagopal & Srinivasa [46]). In this approach, the stress in the fluid is determined from the mapping between the tangent spaces of the natural configuration of the fluid to the current configuration occupied by it. In Fig. 1 this is
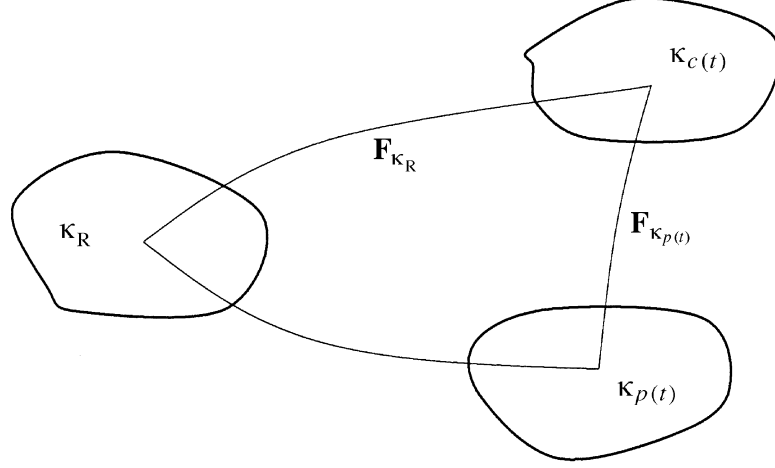
FIG. 1. Natural configurations associated with the fluid.

the mapping between the configurations $\kappa_{p(t)}$ and $\kappa_{c(t)}$. The natural configuration is not fixed as in an elastic solid but evolves as the fluid is subjected to deformation. We will consider viscoelastic fluid models cast into this framework. The stress tensor of a viscoelastic fluid with instantaneous elasticity can be written in the following form:

$$\mathbf{T} = -p\mathbf{I} + \mathbf{f}_{\kappa_{p(t)}}(\mathbf{B}_{\kappa_{p(t)}}), \tag{5}$$

where the left Cauchy–Green stretch tensor is

$$\mathbf{B}_{\kappa_{p(t)}} = \mathbf{F}_{\kappa_{p(t)}}\mathbf{F}_{\kappa_{p(t)}}^T. \tag{6}$$

An evolution equation is prescribed for $\mathbf{B}_{\kappa_{p(t)}}$, i.e.,

$$\overset{\nabla}{\mathbf{B}}_{\kappa_{p(t)}} \equiv \dot{\mathbf{B}}_{\kappa_{p(t)}} - \mathbf{L}\mathbf{B}_{\kappa_{p(t)}} - \mathbf{B}_{\kappa_{p(t)}}\mathbf{L}^T = \mathbf{h}(\mathbf{B}_{\kappa_{p(t)}}), \tag{7}$$

where $\overset{\nabla}{\mathbf{B}}_{\kappa_{p(t)}}$ is the upper-convected Oldroyd derivative, the dot signifies the usual material time derivative, $\mathbf{L}$ is the gradient of velocity, i.e. $\mathbf{L} = \text{grad}\mathbf{v}$, and $\mathbf{h}$ is a tensor valued function of $\mathbf{B}_{\kappa_{p(t)}}$. Equation (7) is tantamount to prescribing the evolution of the underlying natural configuration. Rajagopal & Srinivasa [46] obtain particular forms of $\mathbf{h}$ in (7) by assuming a specific form for the Helmholtz potential, and the rate of dissipation as well as making the additional assumption that the rate of dissipation is maximized. Depending on the functional forms of the Helmholtz potential and the rate of dissipation chosen, a whole range of models can be derived. Rajagopal & Srinivasa [46] derive the constitutive equation for a generalized Maxwell fluid using this procedure. For a Helmholtz potential consistent with that of a neo-Hookean solid, the stress in the fluid is related to $\mathbf{B}_{\kappa_{p(t)}}$ as:

$$\mathbf{T} = -p\mathbf{I} + \mu_f \mathbf{B}_{\kappa_{p(t)}}. \tag{8}$$

The generalized Maxwell fluid proposed by Rajagopal & Srinivasa [46] has an evolution equation for $\mathbf{B}_{\kappa_{p(t)}}$ of the form

$$\overset{\triangledown}{\mathbf{B}}_{\kappa_{p(t)}} = \frac{1}{\lambda} \left(\frac{3}{\text{tr}(\mathbf{B}_{\kappa_{p(t)}}^{-1})} \mathbf{I} - \mathbf{B}_{\kappa_{p(t)}} \right), \tag{9}$$

which upon linearization reduces to the Maxwell fluid. The constitutive equations for a Maxwell fluid in this framework take the form

$$\overset{\triangledown}{\mathbf{B}}_{\kappa_{p(t)}} = \frac{1}{\lambda} \left(\mathbf{I} - \mathbf{B}_{\kappa_{p(t)}} \right), \tag{10}$$

where μ_f and λ are material constants. Models similar to the one in (9) have also been derived by Leonov & Prokunin [31] using non-equilibrium thermodynamics. However, the framework presented in [41] includes a variety of responses, has a more general structure and can deal with symmetry changes, observed, for e.g., in shape memory alloys. Also, the thermo-mechanical framework is quite different, and more importantly, the significance attached to many of the quantities are quite different. In another similar approach, viscoelastic fluids are modelled using an internal variable called the configuration tensor, $\mathbf{C}$. In viscoelastic fluid models based on the configuration tensor, the stress is related to the configuration tensor in the same way as (8), i.e. with $\mathbf{B}_{\kappa_{p(t)}}$ replaced by $\mathbf{C}$. In these models an evolution equation is prescribed for $\mathbf{C}$. More details on these models can be found in Leonov & Prokunin [31]. The main difference between these two approaches is the meaning given to $\mathbf{B}_{\kappa_{p(t)}}$ and $\mathbf{C}$. The tensor $\mathbf{B}_{\kappa_{p(t)}}$ has a specific kinematic meaning, which implies that it satisfies the constraint due to incompressibility, $\det(\mathbf{B}_{\kappa_{p(t)}}) = 1$. The configuration tensor, however, does not satisfy any such constraint. In this work we shall use the Maxwell fluid model to represent the melt. However, any other fluid model developed within the framework of natural configurations can be used instead of the Maxwell fluid model. We shall use the linearized Maxwell fluid model mainly for the sake of simplicity, even though it does not satisfy the constraint $\det(\mathbf{B}_{\kappa_{p(t)}}) = 1$ exactly.

The tensor $\mathbf{B}_{\kappa_{p(t)}}$ contains information about the orientation and stretch in the polymer molecules, albeit in an averaged sense. We shall use this information to determine the orientation of the crystalline solid. Before crystallization can begin, certain activation conditions have to be met. We shall assume that crystallization takes place when the temperature falls below a certain value, the melting temperature. The next step is to model the mixture of a crystalline solid and a viscoelastic fluid. Once crystallization commences, assumptions need to be made about the state in which the solid is formed. Experiments suggest that the crystals have a preferred orientation in the direction in which the molecules in the melt are stretched, this phenomenon has to be accounted for by the model. In the following section we shall discuss the approach used.

3.2   Modeling the fluid to solid transition

Once solidification is initiated, the rate at which it progresses is also prescribed by a rate equation for the mass fraction, α, of the solid phase. The equation commonly used in the literature to characterize the growth of the crystalline phase is the Avrami equation. A particular form of the Avrami equation that is often used is

$$\alpha = A(1 - \exp(-kt^n)), \tag{11}$$

where n is called the Avrami exponent, k is a constant and A is the mass fraction of the crystalline part after crystallization has ceased. The Avrami equation has been modified to include the effects

of the deformation in the polymer melt chain by making the constants k and n functions of the extension in the melt.

A general form of a constitutive equation for the crystallization growth kinetics would be

$$\frac{d\alpha}{dt} = h(\alpha, \mathbf{B}_{\kappa_{p(t)}}, \theta).$$ (12)

Note that (11) can be written in the form of (12) by differentiating with respect to time:

$$\frac{d\alpha}{dt} = Ak^{\frac{1}{n}}n\left(1 - \frac{\alpha}{A}\right)\left[\ln\left(\frac{1}{1 - \alpha/A}\right)\right]^{\frac{n-1}{n}}.$$ (13)

In this work we use the Avrami equation in the form of (13) to determine the rate of crystallization. Here, it should be noted that the Avrami equation has been correlated with experimental data for slow crystallization in a controlled environment. In many processing applications, for e.g., in film blowing, however, the melt is cooled very rapidly and experiments suggest that the rate of crystallization is controlled by the rate at which heat is removed from the melt. Currently, a good understanding of this type of non-equilibrium crystallization is not available and this is an area that needs to be addressed in the future.

We shall treat the fluid–solid mixture as a constrained mixture. As in traditional mixture theory (see Truesdell [57], Bowen [10], Atkin & Craine [2] and Rajagopal & Tao [48]), we allow co-occupancy, in a homogenized sense, of the phases at a point. However, unlike traditional mixture theory both the phases are constrained to have the same displacement, i.e. one phase does not diffuse through the other. This is a reasonable assumption for polymeric materials because the same molecule traverses both the amorphous and crystalline phases and the crystalline phase pins down the molecule preventing it from diffusing. We also assume that the stress at a point is given by a combination of the form

$$\mathbf{T} = p\mathbf{I} + \mathbf{T}_s + \mathbf{T}_f,$$ (14)

where the stress $\mathbf{T}_f$ is given by

$$\mathbf{T}_f = (1 - \alpha)\mathbf{f}_{\kappa_{p(t)}}(\mathbf{B}_{\kappa_{p(t)}}),$$ (15)

$$\overset{\triangledown}{\mathbf{B}}_{\kappa_{p(t)}} = \mathbf{h}(\mathbf{B}_{\kappa_{p(t)}}).$$ (16)

The additive decomposition in (14) can be shown to result naturally within a full thermodynamic framework (see Rao & Rajagopal [49]) if one assumes that the internal energy and entropy for the mixture are additive and an appropriate form of the second law of thermodynamics is used.

Once the fluid begins to solidify, assumptions have to be made about the nature of the solid and the configuration in which the solid is formed. We treat the newly formed solid as an elastic solid, and we suppose that the elastic solid is formed in its stress-free state. This is similar to the approach used by Rajagopal & Wineman [42] for their multi-network theory for polymers. As further deformation takes place this newly formed solid is deformed. The solid that is subsequently formed is also born in a stress-free state. The crystallized solid can be thought of as a mixture of elastic solids with different natural configurations. The stress-free configuration of the solid fraction born at some time t is the configuration of the body at the time t. Solidification is initiated at time t_1 and terminates at t_2. In Fig. 2, let τ be some time later than t_1 at which solidification is taking place. We shall assume that the current stress (at time t) in the body due to the solid fraction born at
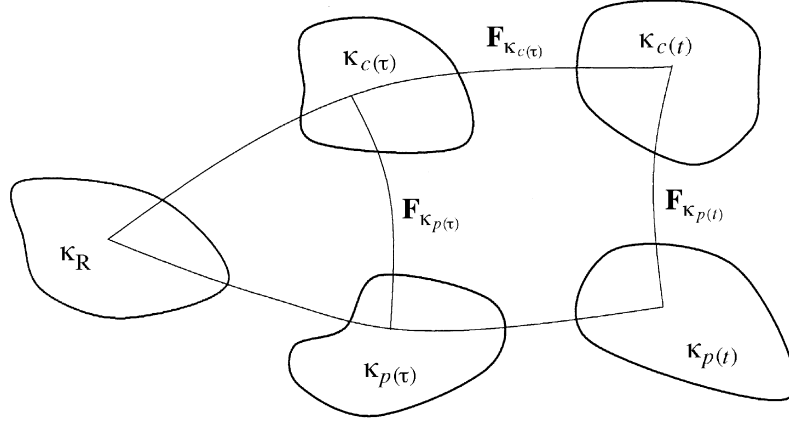
FIG. 2. Natural configurations associated with the crystallizing fluid-solid mixture.

time τ is determined by the deformation gradient from the configuration of the body at time τ and the current configuration at time t, $\mathbf{F}_{\kappa_{c(\tau)}}$, while the stress in the fluid is determined by $\mathbf{F}_{\kappa_{p(t)}}$. Under these assumptions, the equation for the stress in the solid during crystallization is:

$$\mathbf{T}_s = \int_{t_1}^{t} \mathbf{g}_{\kappa_{c(\tau)}}(\mathbf{F}_{\kappa_{c(\tau)}}) \frac{d\alpha}{d\tau} \, d\tau, \tag{17}$$

and if crystallization ceases at time t_2, the stress in the crystalline solid is:

$$\mathbf{T}_s = \int_{t_1}^{t_2} \mathbf{g}_{\kappa_{c(\tau)}}(\mathbf{F}_{\kappa_{c(\tau)}}) \frac{d\alpha}{d\tau} \, d\tau, \tag{18}$$

where the functional form for the stress in the solid formed at time τ, $\mathbf{g}_{\kappa_{c(\tau)}}$, can be that of an anisotropic elastic solid. Also, the anisotropy of this newly formed solid can depend upon the conditions under which it is formed. This aspect of the theory makes it very robust in modelling problems of solidification and phase change where the anisotropy of the newly formed solid depends on the deformation history of the material. The way in which this is built into the model depends on the physical problem under consideration. In this paper we are modelling the problem of crystallization in polymers and will tailor the model to fit the requirements of this problem. In polymers, as we have discussed earlier, the anisotropy in the formed solid depends on the orientation of the molecules in the melt at the time of crystallization. The tensor $\mathbf{B}_{\kappa_{p(\tau)}}$ gives us information about the orientation of the molecules in the melt at time $t = \tau$, albeit in an averaged sense. The three principal directions of $\mathbf{B}_{\kappa_{p(\tau)}}$ gives us the directions of principal stretch in the melt. We use these mutually perpendicular principal directions to determine the directions of anisotropy in the solid. The principal directions can be quantified by any two of the three eigenvectors of $\mathbf{B}_{\kappa_{p(\tau)}}$, viz. $\mathbf{n}_{\kappa_{c(\tau)}}$ and $\mathbf{m}_{\kappa_{c(\tau)}}$. The symmetry group of an orthotropic solid is determined by three mutually perpendicular directions, and it is the form of anisotropy that seems appropriate that the solid will have when formed under conditions of unequal stretch in three principal directions. For this reason, we assume that the elastic solid that is formed at *each instant* is an orthotropic elastic solid. The

three principal directions of the orthotropic solid formed at time $t = \tau$ are determined by $\mathbf{n}_{\kappa_{c(\tau)}}$ and $\mathbf{m}_{\kappa_{c(\tau)}}$ and, in general, can change with time. In this work we assume that the functional form $\mathbf{g}_{\kappa_{c(\tau)}}$ is that for an orthotropic solid with respect to the configuration $\kappa_{c(\tau)}$. We assume the directions $\mathbf{n}_{\kappa_{c(\tau)}}$ and $\mathbf{m}_{\kappa_{c(\tau)}}$ are given by any two of the three principal stretch directions of $\mathbf{B}_{\kappa_{p(\tau)}}$ in order to incorporate the dependence of the orientation of the crystalline solid on the directions of stretch in the melt at the instant of crystallization. We could require the anisotropy to be determined by the symmetry group induced due to the deformation gradient from a configuration in which the material was originally isotropic. This would be the case if the natural configuration associated with the state at which solidification has taken place is obtained by $\mathbf{F}_{\kappa_{p(t)}}^{-1}$. This is however not the case as we assume the current configuration in which the solid is formed is its natural state. It is also possible to decide on the symmetry of the solid that is formed based on the symmetry induced by using Noll's rule for the fluid, but this would be too restrictive in general flows, yielding only materials with trivial symmetry.

The general form of the stress tensor while crystallization is taking place is:

$$\mathbf{T} = -p\mathbf{I} + (1 - \alpha)\mathbf{f}_{\kappa_{p(t)}}(\mathbf{B}_{\kappa_{p(t)}}) + \int_{t_1}^{t} \mathbf{g}_{\kappa_{c(\tau)}}(\mathbf{F}_{\kappa_{c(\tau)}})\frac{\mathrm{d}\alpha}{\mathrm{d}\tau}\,\mathrm{d}\tau, \tag{19}$$

and after crystallization ceases the stress is given by (19) with t_2 replacing t in the limits of the integration.

We want to choose a form for the stress in the solid, $\mathbf{g}_{\kappa_{c(\tau)}}$, that can be derived from a Helmholtz potential for an orthotropic material. The reason for doing this is to ensure that this purely mechanical model will fit into the full thermodynamic model that is being developed (see Rao & Rajagopal [49]). The constitutive equation for the Helmholtz potential for an incompressible orthotropic elastic solid depends on the first two invariants of the right Cauchy–Green stretch tensor, $\mathbf{C}_{\kappa_{c(\tau)}}$, which we denote by I_1, I_2, and the following scalars:

$$\begin{aligned}
J_1 &= \mathbf{n}_{\kappa_{c(\tau)}} \cdot \mathbf{C}_{\kappa_{c(\tau)}}\mathbf{n}_{\kappa_{c(\tau)}}, & K_1 &= \mathbf{m}_{\kappa_{c(\tau)}} \cdot \mathbf{C}_{\kappa_{c(\tau)}}\mathbf{m}_{\kappa_{c(\tau)}}, \\
J_2 &= \mathbf{n}_{\kappa_{c(\tau)}} \cdot \mathbf{C}_{\kappa_{c(\tau)}}\mathbf{n}_{\kappa_{c(\tau)}}, & K_2 &= \mathbf{m}_{\kappa_{c(\tau)}} \cdot \mathbf{C}_{\kappa_{c(\tau)}}\mathbf{m}_{\kappa_{c(\tau)}},
\end{aligned} \tag{20}$$

The most general form of the Helmholtz potential for the elastic solid can then be written as:

$$\psi = \psi(I_1, I_2, J_1, J_2, K_1, K_2), \tag{21}$$

where the invariants depend on t and τ. Choosing a specific form for the function ψ results in a specific form for $\mathbf{g}_{\kappa_{c(\tau)}}$ and hence the form of the stress tensor in the solid. For an elastic solid the stress is given by:

$$\mathbf{T} = -p\mathbf{I} + 2\rho\mathbf{F}_{\kappa_{c(\tau)}}\frac{\partial\psi}{\partial\mathbf{C}_{\kappa_{c(\tau)}}}\mathbf{F}_{\kappa_{c(\tau)}}^{T}. \tag{22}$$

Substituting (21) into (22) and simplifying we obtain the most general form for the stress of an incompressible orthotropic elastic solid:

$$\begin{aligned}
\mathbf{T} = -p\mathbf{I} + 2\rho\Bigg\{ &\frac{\partial\psi}{\partial I_1}\mathbf{B}_{\kappa_{p(\tau)}} - \frac{\partial\psi}{\partial I_2}\mathbf{B}_{\kappa_{p(\tau)}}^{-1} + \mathbf{F}_{\kappa_{c(\tau)}}\left(\frac{\partial\psi}{\partial I_1}\mathbf{n}_{\kappa_{c(\tau)}} \otimes \mathbf{n}_{\kappa_{c(\tau)}}\right. \\
&+ \frac{\partial\psi}{\partial K_1}\mathbf{m}_{\kappa_{c(\tau)}} \otimes \mathbf{m}_{\kappa_{c(\tau)}} + \frac{\partial\psi}{\partial J_2}\left(\mathbf{n}_{\kappa_{c(\tau)}} \otimes \mathbf{C}_{\kappa_{c(\tau)}}\mathbf{n}_{\kappa_{c(\tau)}} + \mathbf{C}_{\kappa_{c(\tau)}}\mathbf{n}_{\kappa_{c(\tau)}} \otimes \mathbf{n}_{\kappa_{c(\tau)}}\right) \\
&+ \left.\frac{\partial\psi}{\partial K_2}\left(\mathbf{m}_{\kappa_{c(\tau)}} \otimes \mathbf{C}_{\kappa_{c(\tau)}}\mathbf{m}_{\kappa_{c(\tau)}} + \mathbf{C}_{\kappa_{c(\tau)}}\mathbf{m}_{\kappa_{c(\tau)}} \otimes \mathbf{m}_{\kappa_{c(\tau)}}\right)\right)\mathbf{F}_{\kappa_{c(\tau)}}^{T}\Bigg\}.
\end{aligned} \tag{23}$$

A specific functional form will have to be chosen that is appropriate for the particular material in question. In this work we assume the following form for the stored energy:

$$\psi = c_1(I_1 - 3) + c_2(J_1 - 1)^2 + c_3(K_1 - 1)^2, \tag{24}$$

and this results in the following functional form for stress:

$$\mathbf{T} = -p\mathbf{I} + 2\rho c_1 \mathbf{B}_{\kappa_{p(\tau)}} + 4\rho \mathbf{F}_{\kappa_{c(\tau)}}(c_2(J_1 - 1)\mathbf{n}_{\kappa_{c(\tau)}} \otimes \mathbf{n}_{\kappa_{c(\tau)}}$$
$$+ c_3(K_1 - 1)\mathbf{m}_{\kappa_{c(\tau)}} \otimes \mathbf{m}_{\kappa_{c(\tau)}})\mathbf{F}^T_{\kappa_{c(\tau)}}. \tag{25}$$

For this material $\mathbf{g}_{\kappa_{c(\tau)}}$ takes the form

$$\mathbf{g}_{\kappa_{c(\tau)}}(\mathbf{F}_{\kappa_{c(\tau)}}) = 2\rho c_1 \mathbf{B}_{\kappa_{c(\tau)}} + 4\rho \mathbf{F}_{\kappa_{c(\tau)}}(c_2(J_1 - 1)\mathbf{n}_{\kappa_{c(\tau)}} \otimes \mathbf{n}_{\kappa_{c(\tau)}}$$
$$+ c_3(K_1 - 1)\mathbf{m}_{\kappa_{c(\tau)}} \otimes \mathbf{m}_{\kappa_{c(\tau)}})\mathbf{F}^T_{\kappa_{c(\tau)}}. \tag{26}$$

The material moduli in (26) can, in general, also depend on the conditions in the melt through the eigenvalues of $\mathbf{B}_{\kappa_{p(\tau)}}$, i.e.,

$$c_i = c_i(\sigma_1, \sigma_2, \sigma_3), \qquad i = 1, 2, 3, \tag{27}$$

where σ_1, σ_2 and σ_3 are the eigenvalues of $\mathbf{B}_{\kappa_{p(\tau)}}$. Since the material is assumed to be incompressible, the product of the three eigenvalues is unity. Note that instead of using the eigenvalues in (27) we can use instead the first two invariants of $\mathbf{B}_{\kappa_{p(t)}}$. We also assume that if all three eigenvalues are distinct, then all three material constants are non-zero and the solid formed at each instant is orthotropic. This is the most restrictive symmetry the newly formed material can have. If two of the eigenvalues are the same and different from the third, then the material formed is transversely isotropic, i.e. c_1 and c_2 are non-zero and c_3 is zero. This assumes that $\mathbf{n}_{\kappa_{c(\tau)}}$ is the eigenvector associated with the eigenvalue that is not equal to the other two eigenvalues. If all three of the eigenvalues are the same, then the solid formed at that instant is isotropic and $c_2 = c_3 = 0$ and c_1 is non-zero.

As crystallization proceeds the remaining amorphous chains lose their mobility, as a part of the polymer molecules are in the crystalline portion and a part in the amorphous portion. Also, as the temperature drops the amorphous chains lose their mobility. Both these effects cause the relaxation time of the amorphous part to increase, till it becomes sufficiently large compared to the time scales pertinent to the problem, i.e. it behaves more like a solid. This effect can be incorporated by making the relaxation time in the fluid model (λ in (10)) to be a function of the mass fraction of the solid, i.e.

$$\lambda = \lambda(\alpha). \tag{28}$$

In general, the relaxation time will also be a function of temperature. When the relaxation time becomes sufficiently large, the stress-free configuration of the melt, i.e. $\kappa_{p(t)}$, does not change with further deformation. Hence the part of the mixture that was the melt now behaves like an elastic solid. If the original fluid was chosen to be a Maxwell fluid, the resultant solid behaves like a neo-Hookean solid. The stress in this mixture of an isotropic and anisotropic solid is given by (19) with the difference that the stress-free configuration, $\kappa_{p(t)}$, of the part that was originally a fluid does not change with time. This completes the modelling of the phase transition and the final solid is a mixture of an isotropic and anistropic elastic solid.

4. Calculations for homogenous deformations

We now study some sample problems involving homogenous deformations to obtain a better understanding of the model that has been developed. The Helmholtz potential used is that in (24) which results in a functional form for $\mathbf{g}_{\kappa_{c(\tau)}}$, given by (26). The melt is assumed to behave like a Maxwell fluid, for which the stress is given by (8). The stress in the fluid–solid mixture is then given by (19) with (26) used for $\mathbf{g}_{\kappa_{c(\tau)}}$ and (8) for the stress in the fluid. With these substitutions, the stress in the fluid–solid mixture reduces to:

$$\mathbf{T} = -p\mathbf{I} + (1-\alpha)\mu_f \mathbf{B}_{\kappa_{p(t)}} + 2\rho \int_{t_1}^{t} c_1 \mathbf{B}_{\kappa_{p(\tau)}} \frac{\mathrm{d}\alpha}{\mathrm{d}\tau}$$

$$+4\rho \int_{t_1}^{t} \left(\mathbf{F}_{\kappa_{c(\tau)}} (c_2(J_1-1)\mathbf{n}_{\kappa_{c(\tau)}} \otimes \mathbf{n}_{\kappa_{c(\tau)}} + c_3(K_1-1)\mathbf{m}_{\kappa_{c(\tau)}} \otimes \mathbf{m}_{\kappa_{c(\tau)}}) \mathbf{F}_{\kappa_{c(\tau)}}^{T} \right) \frac{\mathrm{d}\alpha}{\mathrm{d}\tau} \, \mathrm{d}\tau. \quad (29)$$

We study three different homogenous deformations, viz. simple extension, bi-axial extension and simple shear.

4.1 *Simple extension*

The first deformation we study is simple extension. Simple extension is commonly encountered in polymer processing, for e.g., in fibre spinning, where the polymer melt is spun into fibres by subjecting them to large extensional deformations. In these types of processes, the polymer chains crystallize with their chains parallel to direction of extension imparting high strength in that direction. This type of deformation illustrates the strong dependence of the final material properties on the processing conditions. For simple extension, the solid formed is transversely isotropic and the principal stretch direction does not change as the directions of the unit vector $\mathbf{n}_{\kappa_{c(\tau)}}$ remains constant. We shall neglect the inertial effects in this analysis. The deformation in simple extension for an incompressible material is given by:

$$x = \Lambda(t)X, \qquad y = \frac{1}{\sqrt{\Lambda(t)}}Y, \qquad z = \frac{1}{\sqrt{\Lambda(t)}}Z, \quad (30)$$

where $\Lambda(t)$ is the stretch ratio. The material is being extended in the x-direction. For this flow, $\mathbf{F}_{\kappa_{c(\tau)}}$ is given by

$$\mathbf{F}_{\kappa_{c(\tau)}} = \mathrm{diag} \left(\frac{\Lambda(t)}{\Lambda(\tau)}, \sqrt{\frac{\Lambda(\tau)}{\Lambda(t)}}, \sqrt{\frac{\Lambda(\tau)}{\Lambda(t)}} \right). \quad (31)$$

For this motion, the stress tensor in (29) reduces to:

$$\mathbf{T} = -p\mathbf{I} + \mu_f(1-\alpha)\mathbf{B}_{\kappa_{p(t)}} + 2\rho \int_{t_1}^{t} c_1 \mathrm{diag} \left(\left(\frac{\Lambda(t)}{\Lambda(\tau)} \right)^2, \frac{\Lambda(\tau)}{\Lambda(t)}, \frac{\Lambda(\tau)}{\Lambda(t)} \right) \frac{\mathrm{d}\alpha}{\mathrm{d}\tau} \, \mathrm{d}\tau$$

$$+4\rho \int_{t_1}^{t} c_2 \mathrm{diag} \left(\left(\left(\frac{\Lambda(t)}{\Lambda(\tau)} \right)^2 - 1 \right) \left(\frac{\Lambda(t)}{\Lambda(\tau)} \right)^2, 0, 0 \right) \frac{\mathrm{d}\alpha}{\mathrm{d}\tau} \, \mathrm{d}\tau. \quad (32)$$

Assuming that the lateral surfaces are stress free, the expression for the stress in the direction of extension is

$$T_{11} = (1-\alpha)\mu_f(B_{11} - B_{22}) + 2\rho \int_{t_1}^{t} c_1 \left(\left(\frac{\Lambda(t)}{\Lambda(\tau)} \right)^2 - \frac{\Lambda(\tau)}{\Lambda(t)} \right) \frac{\mathrm{d}\alpha}{\mathrm{d}\tau} \, \mathrm{d}\tau$$

$$+4\rho \int_{t_1}^{t} c_2 \left(\left(\frac{\Lambda(t)}{\Lambda(\tau)} \right)^2 - 1 \right) \left(\frac{\Lambda(t)}{\Lambda(\tau)} \right)^2 \frac{d\alpha}{d\tau}\, dt. \tag{33}$$

B_{ij} in (33) is the ijth component of $\mathbf{B}_{\kappa_{p(t)}}$, and at time t it is obtained by solving the ordinary differential equation for B_{ij}, (10). We shall assume that the mass fraction of the crystallized solid is given as a function of time by the differential form of the Avrami equation, (13). We assume that crystallization starts at a known time. The crystallization equation is then given by

$$\alpha = 0, \qquad\qquad\qquad \text{for } 0 \leqslant t \leqslant t_1$$

$$\frac{d\alpha}{dt} = Ak^{\frac{1}{n}} \left(1 - \frac{\alpha}{A} \right) \left[\ln \left(\frac{1}{1 - \alpha/A} \right) \right]^{\frac{n-1}{n}}, \qquad \text{for } t > t_1, \tag{34}$$

here A is the mass fraction of the crystalline portion of the polymer after crystallization has ceased. The relaxation time λ is assumed to depend on the mass fraction α in the following manner:

$$\lambda = \frac{\lambda_0}{A - \alpha}. \tag{35}$$

As the mass fraction of the crystalline material increases, the relaxation time of the fluid increases, until it starts behaving like an elastic solid. The crystallization of rubber is easily incorporated into this framework by treating the initial amorphous polymer as a elastic solid instead of a fluid. Finally, the stretch ratio $\Lambda(t)$ is assumed to have the form:

$$\Lambda(t) = 1 + t. \tag{36}$$

With the assumptions stated above, the resulting ordinary differential equations are solved using a 4th–5th-order Runge–Kutta method. Figure 3 shows the stress in the direction of extension as a function of time. As the crystallization proceeds the stress rises rapidly. After crystallization ceases the material was then unloaded. From this unloaded condition, the final solid was subjected to uniform extension in the direction of the initial extension and in a direction perpendicular to the initial extension. The stress versus stretch is plotted for these in Fig. 4. The stress increases more rapidly in the direction of initial extension as the material is stronger in that direction due to the formation of a crystalline material that is transversely isotropic. The effect of the induced anisotropy on the mechanical response of the material is made transparent by Fig. 4. Note that in all the graphs, the stress has been non-dimensionalized by the elastic modulus of the fluid, μ_f.

4.2   Extension in two perpendicular directions

Extension in two perpendicular directions is another common deformation encountered in polymer processing, for e.g., in film blowing and sheet forming. In these processing operations, the morphology of the final polymeric solid depends on the extension in each direction. In the case of equal bi-axial extension, the polymer chains in the crystals are oriented equally in all directions in the plane, and hence the solid has transverse isotropy. However, if the stretches are unequal, the orientation of the polymer chains will not be equally distributed. The current framework being developed is capable of handling the above-mentioned situation. We assume a deformation of the form:

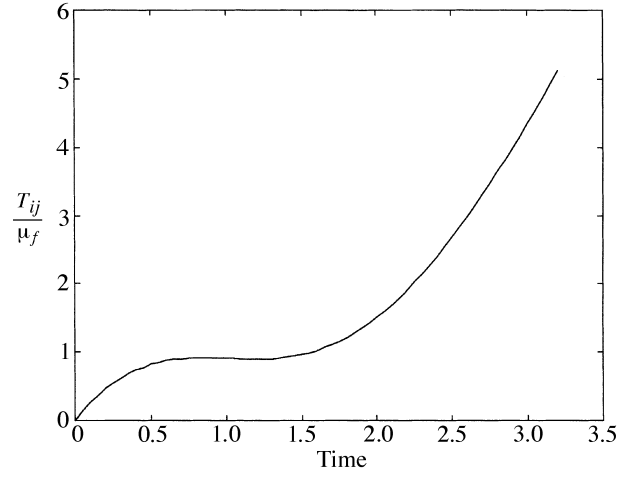$$x = \Lambda_1(t)X, \qquad y = \Lambda_2(t)Y, \qquad z = \frac{1}{\Lambda_1(t)\Lambda_2(t)}Z. \tag{37}$$

FIG. 3. Non-dimensional stress versus time for $\lambda_0 = 0.2s$, $k = 0.5s^{-3}$, $n = 3$, $A = 0.5$, $t_1 = 0.5s$, $\dfrac{\rho c_1}{\mu_f} = 1$ and $\dfrac{4\rho c_2}{\mu_f} = 0.5$
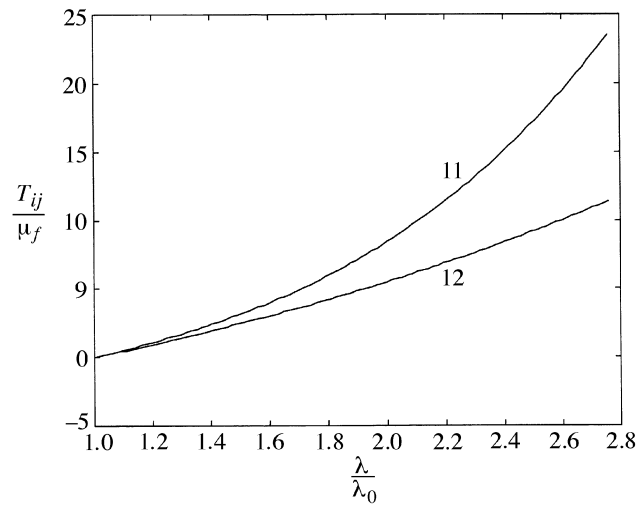

FIG. 4. Non-dimensional stresses in the final solid in the direction of stretch and perpendicular to the direction of stretch for $\lambda_0 = 0.2s$, $k = 0.5s^{-3}$, $n = 3$, $A = 0.5$, $t_1 = 0.5s$, $\dfrac{\rho c_1}{\mu_f} = 1$ and $\dfrac{4\rho c_2}{\mu_f} = 0.5$

For this flow, $\mathbf{F}_{\kappa_{c(\tau)}}$ is given by

$$\mathbf{F}_{\kappa_{c(\tau)}} = \text{diag}\left(\frac{\Lambda_1(t)}{\Lambda_1(\tau)}, \frac{\Lambda_2(t)}{\Lambda_2(\tau)}, \frac{\Lambda_1(\tau)\Lambda_2(\tau)}{\Lambda_1(t)\Lambda_2(t)}\right). \tag{38}$$

For this motion, the stress tensor reduces to;

$$\begin{aligned}
\mathbf{T} = {}& p\mathbf{I} + \mu_f(1-\alpha)\mathbf{B}_{\kappa_{p(t)}} \\
&+ 4\rho \int_{t_1}^t \text{diag}\left(c_2\left(\left(\frac{\Lambda_1(t)}{\Lambda_1(\tau)}\right)^2 - 1\right)\left(\frac{\Lambda_1(t)}{\Lambda_1(\tau)}\right)^2, \quad c_3\left(\left(\frac{\Lambda_2(t)}{\Lambda_2(\tau)}\right)^2 - 1\right)\left(\frac{\Lambda_2(t)}{\Lambda_2(\tau)}\right)^2, 0\right)\frac{d\alpha}{d\tau}\, d\tau \\
&+ 2\rho \int_{t_1}^t c_1 \text{diag}\left(\left(\frac{\Lambda_1(t)}{\Lambda_1(\tau)}\right)^2, \left(\frac{\Lambda_2(t)}{\Lambda_2(\tau)}\right)^2, \left(\frac{\Lambda_1(\tau)\Lambda_2(\tau)}{\Lambda_1(t)\Lambda_2(t)}\right)^2\right)\frac{d\alpha}{d\tau}\, d\tau.
\end{aligned} \tag{39}$$

Assuming that the lateral surface perpendicular to the directions in which extension is taking place is stress free, the expression for the stress in the two directions along which the material is extended is

$$\begin{aligned}
T_{11} = {}& (1-\alpha)\mu_f(B_{11} - B_{33}) + 2\rho \int_{t_1}^t c_1\left(\left(\frac{\Lambda_1(t)}{\Lambda_1(\tau)}\right)^2 - \left(\frac{\Lambda_1(\tau)\Lambda_2(\tau)}{\Lambda_1(t)\Lambda_2(t)}\right)\right)\frac{d\alpha}{d\tau}\, d\tau \\
&+ 4\rho \int_{t_1}^t c_2\left(\left(\frac{\Lambda_1(t)}{\Lambda_1(\tau)}\right)^2 - 1\right)\left(\frac{\Lambda_1(t)}{\Lambda_1(\tau)}\right)^2 \frac{d\alpha}{d\tau}\, d\tau,
\end{aligned} \tag{40}$$

$$\begin{aligned}
T_{22} = {}& (1-\alpha)\mu_f(B_{22} - B_{33}) + 2\rho \int_{t_1}^t c_1\left(\left(\frac{\Lambda_2(t)}{\Lambda_2(\tau)}\right)^2 - \left(\frac{\Lambda_1(\tau)\Lambda_2(\tau)}{\Lambda_1(t)\Lambda_2(t)}\right)\right)\frac{d\alpha}{d\tau}\, d\tau \\
&+ 4\rho \int_{t_1}^t c_3\left(\left(\frac{\Lambda_2(t)}{\Lambda_2(\tau)}\right)^2 - 1\right)\left(\frac{\Lambda_2(t)}{\Lambda_2(\tau)}\right)^2 \frac{d\alpha}{d\tau}\, d\tau.
\end{aligned} \tag{41}$$

We shall assume that (34) and (35) for the mass fraction and the relaxation time are the same. We further assume the following specific forms for Λ_1 and Λ_2

$$\Lambda_1 = K_1 t + 1, \qquad \Lambda_2 = K_2 t + 1. \tag{42}$$

When $K_1 = K_2$ the deformation reduces to equal bi-axial extension. Figure 5 shows the stresses for the two in plane directions plotted against time for equal bi-axial extension. Since the extension is equal in both the directions ($K_1 = K_2 = 1.5$), the crystalline phase formed is transversely isotropic with axis of symmetry being the z-direction perpendicular to the plane in which the material is being subjected to the bi-axial extensions and the stresses in the other two directions are equal. Figure 6 shows the stress in the two in plane directions for unequal bi-axial extensions. In this case, the values for K_1 and K_2 were chosen to be $K_1 = 1.5$ and $K_2 = 1.0$. The crystalline phase formed in this case is orthotropic.
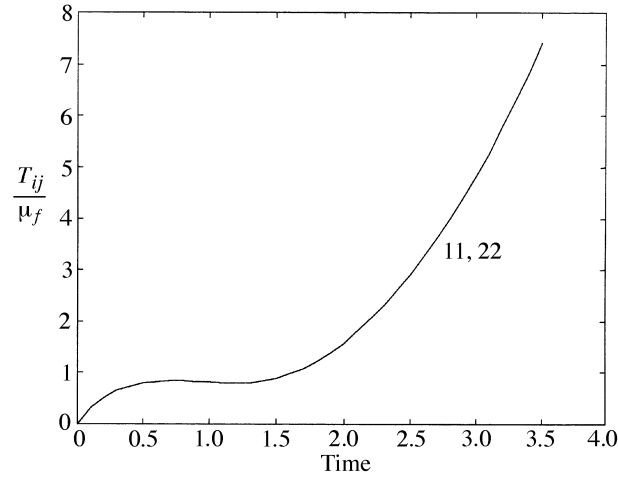
FIG. 5. Non-dimensional stresses versus time for equal bi-axial extension for $\lambda_0 = 0.2s$, $K_1 = K_2 = 1.5s^{-1}$, $k = 0.8s^{-3}$, $n = 3$, $A = 0.5$, $t_1 = 0.5s$, $\dfrac{\rho c_1}{\mu_f} = 0.5$, $4\dfrac{\rho c_2}{\mu_f} = 0.5$ and $4\dfrac{\rho c_3}{\mu_f} = 0.5$
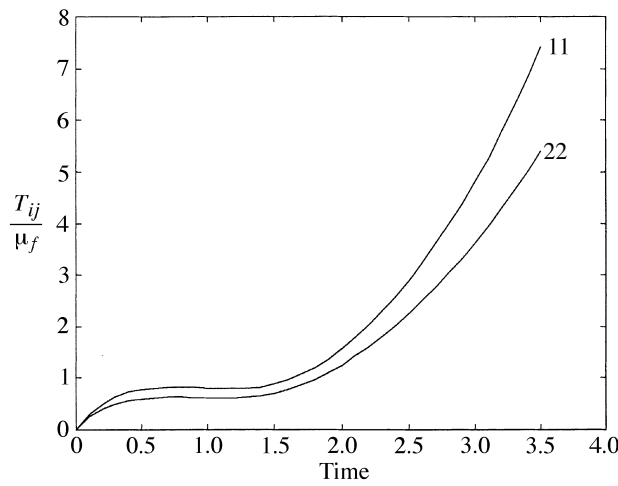

FIG. 6. Non-dimensional stresses versus time for equal bi-axial extension for $\lambda_0 = 0.2s$, $K_1 = 1.5s^{-1}$, $K_2 = 1.0s^{-1}$, $k = 0.8s^{-3}$, $n = 3$, $A = 0.5$, $t_1 = 0.5s$, $\dfrac{\rho c_1}{\mu_f} = 0.5$, $4\dfrac{\rho c_2}{\mu_f} = 0.5$ and $4\dfrac{\rho c_3}{\mu_f} = 0.5$

4.3   *Simple shear*

Crystallization in the case of simple shear is different from extensional flows in that the principal stretch directions constantly change with time. Experiments indicate (Haas & Maxwell [20] and Eder *et al.* [13]) that at sufficiently high shear rates a high degree of anisotropy was observed in the crystallized sample. This feature can be captured in the current framework through two of the eigenvectors of $\mathbf{B}_{\kappa_{p(\tau)}}$, $\mathbf{n}_{\kappa_{c(\tau)}}$ and $\mathbf{m}_{\kappa_{c(\tau)}}$, which are changing in a simple shear flow, and which will tend to align towards the direction of flow and perpendicular to the direction of flow for a sufficiently high shear rate. The deformation for simple shear is of the form:

$$x = X + k(t)Y, \qquad y = Y, \qquad z = Z. \tag{43}$$

For this flow, $\mathbf{F}_{\kappa_{c(\tau)}}$ is given by

$$\mathbf{F}_{\kappa_{c(\tau)}} = \begin{pmatrix} 1 & \Delta k & 0 \\ 0 & 1 & 0 \\ 0 & 0 & 1 \end{pmatrix}, \tag{44}$$

where $\Delta k = k(t) - k(\tau)$. Once again the stress tensor is given by (29). For this flow the two eigenvectors of $\mathbf{B}_{\kappa_{p(\tau)}}$, $\mathbf{n}_{\kappa_{c(\tau)}}$ and $\mathbf{m}_{\kappa_{c(\tau)}}$ are in the x–y plane and the third eigenvector is perpendicular to x–y plane and is the unit vector in the z-direction. Define $\mathbf{n}_{\kappa_{c(\tau)}}$ and $\mathbf{m}_{\kappa_{c(\tau)}}$ through:

$$\mathbf{n}_{\kappa_{c(\tau)}} = \begin{pmatrix} a \\ b \\ 0 \end{pmatrix}, \qquad \mathbf{m}_{\kappa_{c(\tau)}} = \begin{pmatrix} c \\ d \\ 0 \end{pmatrix}. \tag{45}$$

In the above equations, a, b, c and d are functions of τ and are determined from the eigenvectors of $\mathbf{B}_{\kappa_{p(\tau)}}$. The invariants J_1 and K_1 in (20) can be expressed as:

$$\begin{aligned} J_1 &= a^2 + 2\Delta kab + (1 + \Delta k^2)b^2, \\ K_1 &= c^2 + 2\Delta kcd + (1 + \Delta k^2)d^2. \end{aligned} \tag{46}$$

For this flow we assume that the stress in the z-direction is constant, i.e. solving (29) for p in terms of the stress in the z-direction

$$-p = T_{33} - (1 - \alpha)\mu_f - 2\rho \int_{t_1}^{t} c_1 \frac{\mathrm{d}\alpha}{\mathrm{d}\tau} \, \mathrm{d}\tau. \tag{47}$$

Solving for the other non-zero stress components using (29), (44), (45), (46) and (47) we obtain:

$$\begin{aligned} T_{11} = {}&(T_{33} - (1 - \alpha)\mu_f) + (1 - \alpha)\mu_f B_{11} + 2\rho \int_{t_1}^{t} c_1 \Delta k^2 \frac{\mathrm{d}\alpha}{\mathrm{d}\tau} \, \mathrm{d}\tau \\ &+ 4\rho \int_{t_1}^{t} \left[c_2(J_1 - 1)(a^2 + 2\Delta kab + b^2 \Delta k^2) \right] \frac{\mathrm{d}\alpha}{\mathrm{d}\tau} \, \mathrm{d}\tau \\ &+ 4\rho \int_{t_1}^{t} \left[c_3(K_1 - 1)(c^2 + 2\Delta kcd + d^2 \Delta k^2) \right] \frac{\mathrm{d}\alpha}{\mathrm{d}\tau} \, \mathrm{d}\tau \end{aligned} \tag{48}$$

$$\begin{aligned} T_{22} = {}&(T_{33} - (1 - \alpha)\mu_f) + (1 - \alpha)\mu_f B_{22} + 4\rho \int_{t_1}^{t} \left[c_2(J_1 - 1)b^2 \right] \frac{\mathrm{d}\alpha}{\mathrm{d}\tau} \, \mathrm{d}\tau \\ &+ 4\rho \int_{t_1}^{t} \left[c_3(K_1 - 1)d^2 \right] \frac{\mathrm{d}\alpha}{\mathrm{d}\tau} \, \mathrm{d}\tau, \end{aligned} \tag{49}$$
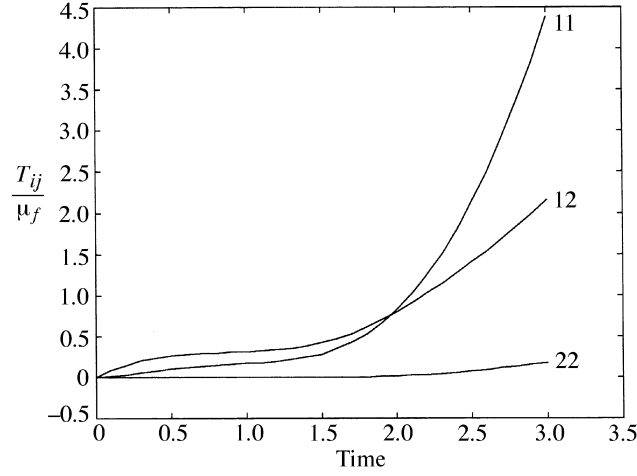
FIG. 7. Non-dimensional stresses versus time for simple shear for $\lambda_0 = 0.2s$, $K = 1.0s^{-1}$, $k = 0.5s^{-3}$, $n = 3$, $A = 0.6$, $t_1 = 0.5s$, $\dfrac{\rho c_1}{\mu_f} = 0.5$, $4\dfrac{\rho c_2}{\mu_f} = 0.3$ and $4\dfrac{\rho c_3}{\mu_f} = 0.3$

$$T_{12} = (1 - \alpha)\mu_f)B_{12} + 2\rho \int_{t_1}^{t} c_1 \Delta k \frac{d\alpha}{d\tau} + 4\rho \int_{t_1}^{t} \left[c_2(J_1 - 1)(ab + \Delta kb^2) \right] \frac{d\alpha}{d\tau}\, d\tau$$

$$+4\rho \int_{t_1}^{t} \left[c_3(K_1 - 1)(cd + \Delta kd^2) \right] \frac{d\alpha}{d\tau}\, d\tau. \tag{50}$$

For the purpose of illustration we shall assume that $k(t)$ is a linear function of time, i.e.

$$k(t) = Kt. \tag{51}$$

We shall assume that (34) and (35) for the mass fraction and the relaxation time are the same. With these assumptions, the equations were solved and the two components of the stress are plotted against time in Fig. 7. As in the other two cases, growth in the stress is rapid after crystallization is completed and at high levels of shear T_{11} grows more rapidly than T_{12}.

5. Conclusions

In this paper we have developed a model using the framework of multiple natural configurations to capture the effects observed during crystallization in polymers as the material evolves from a fluid-like response to a solid-like response. The model is capable of capturing the evolving anisotropy of the crystalline phase as it is formed. The induced anisotropy of the crystalline phase is determined by the deformation of the melt and this is borne out by the results depicted in Figs 4, 6 and 7. However, in order to make comparisons with the predictions from experiments, it is necessary to take into account thermodynamic considerations. Such an analysis, which studies the problem of crystallization from a fully thermodynamic framework, is being carried out by Rao & Rajagopal [50]. Here, Rao & Rajagopal [50] simulate crystallization during the stretching of polyethylene

terephthalate films. Preliminary results indicate very good agreement between the experimental data and the predictions of the model.

REFERENCES

1. ASTARITA, G. & KENNY, J. M. The Stefan and Deborah numbers in polymer crystallization. *Chem. Eng. Commun.* **53**, (1987) 69.
2. ASTARITA, G. & MARUCCI, G. *Principles of Non-Newtonian Fluid Mechanics.* McGraw-Hill, New York (1974).
3. ATKIN, R. J. & CRAINE, R. E. Continuum theory of mixtures: basic theory and historical development. *Q. J. Mech. Appl. Math.* **29**, (1976) 209.
4. AVRAMI, M. Kinetics of phase change. *J. Chem. Phys.* **7**, (1939) 1103.
5. AVRAMI, M. Kinetics of phase change. *J. Chem. Phys.* **8**, (1940) 212.
6. AVRAMI, M. Kinetics of phase change. *J. Chem. Phys.* **9**, (1941) 177.
7. BALDONI, F. & RAJAGOPAL, K. R. A continuum theory for the thermomechanics solidification. *Int. J. Non-Linear Mech.* **32**, (1997) 3.
8. BANKOFF, S. G. Heat conduction or diffusion with phase change. *Adv. Chem. Eng.* **5**, (1964) 75.
9. BERGER, J. & SCHNEIDER, W. Models of rate controlled solidification. *Plast. Rubber Process. Appl.* **6**, (1986) 127.
10. BOWEN, R. M. Theory of mixtures. In Eringen, A. C. (ed.), *Continuum Physics* vol. III. Academic Press, New York (1975).
11. CRANK, J. *Free and Moving Boundary Problems.* Clarendon Press, Oxford (1984).
12. DOI, M. & EDWARDS, S. F. *The Theory of Polymer Dynamics.* Oxford Science Publications, Oxford (1986).
13. EDER, G., JANSESCHITZ-KRIEGL, H., & LIEDAUER, S. Crystallization processes in quiescent and moving polymer melts under heat transfer conditions. *Prog. Polym. Sci.* **15**, (1990) 629.
14. EDER, G. JANSESCHITZ-KRIEGL, H., & KROBATH, G. Shear induced crystallization, a relaxation phenomenon in melts. *Prog. Colloid Polym. Sci.* **80**, (1989) 1.
15. FASANO, A. & PRIMICERIO, M. Free boundary problems for nonlinear equations with nonlinear free boundary conditions. *J. Math. Anal. Appl.* **72**, (1979) 247.
16. FLORY, P. J. Thermodynamics of crystallization in high polymers I. Crystallization induced by stretching. *J. Chem. Phys.* **15**, (1947) 397.
17. GAYLORD, R. J. & LOHSE, D. J. Morphological changes during oriented polymer crystallization. *Polym. Eng. Sci.* **16**, (1976) 163.
18. GAYLORD, R. J. A theory of stress induced crystallization of cross linked polymer networks. *J. Polym. Sci.* **14**, (1976) 1827.
19. GLICKSMAN, M. E., CORRIELL, S. R., & MCFADDEN, G. B. Interaction of flows with the crystal melt interface. *Annu. Rev. Fluid Mech.* **18**, (1986) 307.
20. HAAS, T. W. & MAXWELL, B. Effects of shear stress on the crystallization of linear polyethylene and polybutene-1. *Polym. Eng. Sci.* **9**, (1969) 225.
21. JANSESCHITZ-KRIEGL, H., EDER, G., KROBATH, G., & LIEDAUER, S. The Stefan problem in polymer processing: theory and experimentation. *J. Non-Newton. Fluid Mech.* **23**, (1987) 107.
22. JOHNSON, G. A., LIVESAY, G. A., WOO, S. L. Y., & RAJAGOPAL, K. R. A single integral finite strain viscoelastic model of ligaments and tendons. *J. Bioeng.* **118**(2), (1996) 221.
23. KATAYAMA, K., MURAKAMI, S., & KOBAYASHI, K. An apparatus for measuring flow induced crystallization in polymers. *Bull. Inst. Chem. Res. Kyoto Univ.* **54**, (1976) 82.

24. KAWAI, T., IGUCHI, M., & TONAMI, H. Crystallization of polyethylene under molecular orientation. *Kolloid-Z.* **221**, (1969) 38.

25. KELLER, A. & MACHIN, M. J. Direct evidence for distinctive, stress induced nucleus crystals in the crystallization of oriented polymer melts. *J. Macromol. Sci.-Phys.* **B3**, (1969) 153.

26. KOBAYASHI K. & NAGASAWA T. Crystallization of sheared polymer melts. *J. Macromol. Sci.-Phys.* **B4**, (1970) 331.

27. KROBATH, G., LIEDAUER, S., & JANSESSCHITZ-KRIEGL, H. Crystallization fronts in quenched polymer samples. *Polym. Bull.* **14**, (1985) 1.

28. LAGASSE, R. R. & MAXWELL, B. An experimental study of the kinetics in polymer crystallization during shear flow. *Polym. Eng. Sci.* **16**, (1976) 189.

29. LAMÉ, M. M. & CLAPEYRON, B. P. E. Memoire sur la solidification par refroidissement d'un globe liquide. *Ann. Chim. Phys.* **47**, (1831) 250.

30. LANDAU, L. D. Collected Papers, Gordon Breach (1967).

31. LEONOV, A. I. & PROKUNIN, A. N. *Nonlinear Phenomenon, Flow of Viscoelastic Polymer Fluids.* Chapman & Hall, New York (1994).

32. MACKLEY, M. R., & KELLER, A. Flow induced crystallization in polyethylene melts. *Polymer* **14**, (1973) 16.

33. MACKLEY, M. R., FRANK, F. C., & KELLER, A. Flow induced crystallization in polyethylene melts. *J. Mat. Sci.* **10**, (1975) 1501.

34. MALKIN, A. YA., BEGHISHEV, V. P., KEAPIN, I. A., & BOLGOV, S. A. General treatment of polymer crystallization kinetics—Part 1. A new macrokinetic equation and its experimental verification. *Polym. Eng. Sci.* **24**, (1984) 1396.

35. MALKIN, A. YA., BEGHISHEV, V. P., KEAPIN, I. A., & ANDRIANOVA, Z. S. General treatment of polymer crystallization kinetics—Part 1.2 Kinetics of non-isothermal crystallization. *Polym. Eng. Sci.* **24**, (1984) 1402.

36. MANDELKERN, L. *Crystallization of Polymers.* McGraw Hill, New York (1964).

37. McHUGH, A. J. Flow induced crystallization in polymers. In Lyngaae-Jorgenson, J. & Sandergaard, K. (eds), *Rheo-physics of Multiphase Polymeric Systems*, Technomic Publishing Co., Lancaster, PA (1995), p. 227.

38. McHUGH, A. J., GUY, R. K., & TREE, D. A. Extensional flow-induced crystallization of a polyethylene melt. *Colloids Polym Sci* **271**, (1993) 629.

39. NOGAMI, K., MURAKAMI, S., KATAYAMA, K., & KOBAYASHI, K. An optical study on shear-induced crystallization in polymers. *Bull. Inst. Chem. Res. Kyoto Univ.* **55**, (1977) 277.

40. PETERLIN, A. Crystallization from a strained melt. *Polym. Eng. Sci.* **16**, (1976) 126.

41. RAJAGOPAL, K. R. On constitutive relations and material modelling (in preparation).

42. RAJAGOPAL, K. R. & WINEMAN, A. S. A constitutive equation for nonlinear solids which undergo deformation induced microstructural changes. *Int. J. Plast.* **8**, (1992) 385–395.

43. RAJAGOPAL, K. R. & SRINIVASA, A. S. Inelastic behaviour of materials: Part-I—Theoretical underpinnings. *Int. J. Plast.* **14**, (1998) 945.

44. RAJAGOPAL, K. R. & SRINIVASA, A. S. On the inelastic behaviour of solids: Part-I—Twinning. *Int. J. Plast.* **11**, (1995) 653.

45. RAJAGOPAL, K. R. & SRINIVASA, A. S. On the thermodynamics of shape memory wires. *ZAMP* **50**, (1999) 459.

46. RAJAGOPAL, K. R. & SRINIVASA, A. S. A thermodynamic framework for rate type fluid models. *J. Non-Newton. Fluid Mech.* (in press).

47. RAJAGOPAL, K. R. & SRINIVASA, A. S. Modeling of anisotropic fluids (in preparation).

48. RAJAGOPAL, K. R. & TAO, L. *Mechanics of Mixtures.* World Scientific, New Jersey (1995).

49. RAO , I. J. & RAJAGOPAL, K. R. A continuum theory for crystallization in polymers (in preparation).

50. RAO, I. J. & RAJAGOPAL, K. R. A study of strain induced crystallization in polymers, *Intl J. of Solids and Structures* (in press).

51. RUBINSTEIN, L. I. *The Stefan Problem*. AMS Translations of Mathematics Monographs 27. American Mathematical Society, Providence, RI (1971).

52. SCHULTZ, J. M. Theory of crystallization in high-speed spinning. *Polym. Eng. Sci.* **31**, (1991) 661.

53. SHERWOOD, C. H., PRICE, F. P., & STEIN, R. S. The effects of shear on the crystallization kinetics of poly(ethylene oxide) and poly(ε-caprolactone) melts. *J. Polym. Sci. Polym. Symp.* **63**, (1978) 77.

54. SMITH, K. J. Crystalline growth due to stress induced nucleation. *Polym. Eng. Sci.* **16**, (1976) 169.

55. SMITH, K. J. Inclusion of mobile crosslinks and lateral crystalline growth in the theory of stress induced crystallization. *J. Polym. Sci.* B**21**, (1983) 45.

56. STEFAN, J. On the theory of formation of ice, in particular in the polar sea. *Ann. Phys. Chem. (Wiedemann)* **42**, (1891) 269.

57. TRUESDELL, C. Sulle Basi Della Termomeccanica. *Rend. Lincei* **22**, (1957) 33–38.

58. ULRICH, R. E. & PRICE F. P. Morphology development during shearing of poly(ethylene oxide) melts. *J. Appl. Polym. Sci.* **20**, (1976) 1077.

59. VAN DER VEGT, A. K. & SMIT, P. P. A. Crystallization phenomenon in flowing polymers. *Soc. Chem. Ind.* **26**, (1967) 313.

60. WARD, I. M. & HADLEY, D. W. *An Introduction to the Mechanical Properties of Solid Polymers*. John Wiley & Sons, New York (1993).

61. WHITE, J. L. Structure development in polymer processing. *Pure Appl. Chem.* **55**, (1983) 765.

62. WHITE, J. L. & SPRUIELL, J. E. The specification of orientation and its development in polymer processing. *Polym. Eng. Sci.* **23**, (1983) 247.

63. WOLCOWICZ, M. D. Nucleation and crystal growth in sheared poly(1-butene) melts. *J. Polym. Sci. Polym. Symp.* **63**, (1978) 365.

64. ZIABICKI, A. Theoretical analysis of oriented and non-isothermal crystallization. I. Phenomenological considerations. Isothermal crystallization accompanied by similtaneous orientation or disorientation. *Colloid Polym. Sci.* **252**, (1974) 207.

65. ZIABICKI, A. Crystallization of polymers in variable external conditions. *Colloid Polym. Sci.* **274**, (1996) 209.